Anna De Grassi   ORCID iD: 0000-0001-7273-4263

CRAT missense variants cause abnormal carnitine acetyltransferase function in an early-onset case of Leigh syndrome.

Authors: Luna Laera[1,§], Giuseppe Punzi[1,§], Vito Porcelli[1], Nicola Gambacorta[1], Lucia Trisolini[1], Ciro L. Pierri[1], Anna De Grassi[1,*]

Affiliations: [1]Department of Biosciences, Biotechnology and Biopharmaceutics, University of Bari, Bari, Italy.

[§]These authors should be regarded as joint First Authors

[*]**Correspondence**

Anna De Grassi, Dept. of Biosciences, Biotechnology and Biopharmaceutics, University of Bari, via Orabona 4, 70125, Bari, Italy. Email: anna.degrassi@uniba.it

Abstract

Leigh syndrome, or subacute necrotizing encephalomyelopathy, is one of the most severe pediatric disorders of the mitochondrial energy metabolism. By performing whole-exome sequencing in a girl affected by Leigh syndrome and her parents, we identified two heterozygous missense variants (p.Tyr110Cys and p.Val569Met) in the carnitine acetyltransferase (*CRAT*) gene, encoding an enzyme involved in the control of mitochondrial short-chain acyl-CoA concentrations. Biochemical assays revealed carnitine acetyltransferase deficiency in the proband-derived fibroblasts. Functional analyses of recombinant-purified CRAT proteins demonstrated that both missense variants, located in the acyl-group binding site of the enzyme, severely impair its catalytic function toward acetyl-CoA, and the p.Val569Met variant also toward propionyl-CoA and octanoyl-CoA. Although a single recessive variant in *CRAT* has been recently associated with neurodegeneration with brain iron accumulation, our study reports the first kinetic analysis of naturally occurring *CRAT* variants and demonstrates the genetic basis of carnitine acetyltransferase deficiency in a case of mitochondrial encephalopathy.

Keywords: Leigh syndrome, mitochondrial encephalopathy, carnitine acetyltransferase, CRAT.

Main Text

Leigh syndrome is a progressive neurodegenerative disease and the most common pediatric presentation of mitochondrial disorders. Clinical features of Leigh syndrome are extremely heterogeneous, yet stringent diagnostic criteria entail brainstem and/or basal ganglia dysfunction, intellectual and motor developmental delay and evidence

of abnormal energy metabolism, mostly supported by elevated lactate in serum or cerebrospinal fluid (Rahman et al., 1996). Albeit biochemical defects in Leigh syndrome can be classified into two main groups, i.e. isolated or combined deficiency of the mitochondrial respiratory chain (RC) and pyruvate dehydrogenase complex (PDH) deficiency (MIM# 256000), almost one hundred disease genes have been associated with this clinical condition (Lake, Compton, Rahman, & Thorburn, 2016). This remarkable genetic heterogeneity is due to the vast repertoire of gene functions that contribute to mitochondrial energy production, either directly or indirectly, and whose impairment can variably impact on disease presentations and life expectancy (Ruhoy & Saneto, 2014).The carnitine-dependent system includes L-carnitine, a conditionally essential nutrient, and the family of carnitine acyltransferase enzymes, which catalyze the reversible exchange of acyl groups between CoA and carnitine (Jogl, Hsiao, & Tong, 2004). Since acylcarnitines can traverse cellular membranes, differently from their acyl-CoA precursors, the carnitine system impacts the intracellular and the inter-tissue carbon trafficking for a wide spectrum of reactions that are essential for mitochondrial energy production (Ramsay & Zammit, 2004). The mitochondrial CRAT enzyme is the only member of the carnitine acyltransferase family to be active toward short-chain acyl groups ranging from two to four carbon atoms (C2 to C4)(Bloisi et al., 1990), since the peroxisomal carnitine octanoyltransferase (CROT) and the mitochondrial carnitine palmitoyltransferases (CPT1 and CPT2) only act on medium-chain acyl groups (C4 to C10)(Sitheswaran, Price, & Ramsay, 2005) and long-chain acyl groups (C8 to C18)(Schaefer, Jackson, Taroni, Swift, & Turnbull, 1997), respectively.

Here we report a sporadic case of severe early-onset mitochondrial encephalopathy, in which we identified compound heterozygous missense variants in the *CRAT* gene, and performed cellular and *in vitro* functional studies.

This research was approved by the Ethics Committee of the Fondazione IRCCS Istituto Neurologico "C. Besta", Italy, and informed consent was signed by the proband's parent. The proband is a 9-year-old only child of unrelated healthy parents. Starting from the first months of age, she experienced a subacute psychomotor regression showing a typical clinical and neurological presentation of Leigh syndrome, also associated with high levels of serum lactate (see detailed case description and metabolic workup in Supplementary Material and Methods). Mitochondrial RC defects were observed in the proband skeletal muscle by two independent Institutes, although the first Institute reported a partially lowered activity of Complex I and IV, while the second Institute indicated a major deficiency of Complex I (Supp. Table S1). A moderate increase in the level of plasma short-chain acylcarnitines was also observed, which depends on acetylcarnitine (Supp. Table S2). Whole-mitochondrial-genome Sanger sequencing excluded the presence of pathogenic variants in the proband mitochondrial DNA. Exome sequencing was performed on the genomic DNA of the proband and her parents (see Supplementary Material and Methods), with a minimum on-target coverage 70× for 22,000 genes. The sequence variants affecting protein coding sequences or RNA splicing sites were retained if they presented a minor allele frequency ≤ 0.005 in the ExAC database (http://exac.broadinstitute.org), and were analyzed according to all modes of transmissions, i.e. *de novo* variants (dominant) and homozygous or compound heterozygous variants (recessive). Albeit no further filters were applied, the only candidate gene encoding a mitochondria-targeted protein (Supp. Figure S1) was

CRAT (NM_000755.4), which carried the heterozygous nucleotide transitions c.329A>G, p.Tyr110Cys, of paternal origin and c.1705G>A, p.Val569Met, of maternal origin (Figure 1A). The former and the latter are annotated in the dbSNP database (https://www.ncbi.nlm.nih.gov/projects/SNP/) with accessions rs141970897 and rs762425351, respectively, and in the ExAC database with minor allele frequency 0.0011 and 0.0001, respectively. The proband genotype has been submitted to the NCBI ClinVar database (www.ncbi.nlm.nih.gov/clinvar/, with identifiers 617561 and 617562 for c.1705G>A and c.329A>G, respectively). Both CRAT p.Tyr110 and p.Val569 are conserved throughout vertebrate evolution (Supp. Figure S2). The former is also a target of tyrosine phosphorylation in human cells (Supp. Figure S2A), while the latter corresponds to the CPT2 p.Val605 residue, whose variation causes CPT2 deficiency (Supp. Figure S2B).

The analysis of CRAT transcripts, conducted on cDNA prepared from the proband-derived fibroblasts, did not reveal any abnormality in the RNA sequence length (Figure 1B) and detected both the wild-type and the variant alleles (Figure 1C), ruling out a possible effect of the missense variants on gene expression and RNA splicing. Similarly, immunoblotting analysis of cultured-fibroblast lysates excluded a damaging effect of *CRAT* variants on protein content (Figure 1D). Spectrophotometric assays conducted on the same samples (see Supplementary Material and Methods and Figure 1E) instead revealed a markedly reduced carnitine acetyltransferase activity in fibroblasts from the proband, which amount to 10.3% of the activity in control fibroblasts (Figure 1F). *In vitro* enzymatic assays were performed to rule out the possibility that the carnitine acetyltransferase deficiency observed in the proband's cells was due to inter-individual variability or secondary alterations, and to determine the functional consequence of each of the two missense variants of the CRAT protein,

separately. The recombinant polyhistidine-tagged wild-type CRAT and each of the two CRAT variations, generated by site-directed mutagenesis, were expressed in *E. coli* and purified using affinity chromatography (see Supplementary Material and Methods and Supp. Figure S3). The enzyme activity of recombinant CRAT proteins was tested at several concentrations (7.5-150 μM) of acetyl-CoA (C2-CoA), i.e. the most abundant CRAT-specific substrate in mitochondria, of propionyl-CoA (C3-CoA), i.e. another short-chain CRAT-specific substrate, and of octanoyl-CoA (C8-CoA), i.e. a medium-chain nonspecific substrate of CRAT. The activities of each recombinant enzyme followed a classical Michaelis-Menten kinetics model (Figure 2A), which permitted to calculate the maximum activity rate (V_{max}) and the Michaelis-Menten constant (K_m) of CRAT proteins toward each substrate. The CRAT p.Tyr110Cys variant primarily impacted on acetyl-CoA, reducing the V_{max} toward C2-CoA, C3-CoA and C8-CoA to 32%, 45% and 61% of wild-type V_{max} (Figure 2B). The CRAT p.Val569Met variant instead impacted on all the substrates, irrespective of their chain-length, reducing the V_{max} of C2-CoA, C3-CoA and C8-CoA to 24%, 29% and 27%, respectively, of wild-type V_{max} (Figure 2B). Further, both CRAT variants significantly reduced the K_m values toward C2-CoA and toward C8-CoA, but not toward C3-CoA, compared to wild-type (Figure 2C and Supp. Table S3).

The analysis of the CRAT protein structure revealed that both p.Tyr110 and p.Val569, substituted by a sulfur-containing amino acid in the proband, locate within the protein active-site tunnel on the opening side used for binding carnitine/acylcarnitine (Figure 2D). The remodeling of the CRAT protein structure, obtained after replacing each wild-type amino acid residue with the variant residue (see Supplementary Material and Methods), resulted in a global reshape of the amino acids participating to the binding of acyl groups (Figure 2E). The CRAT p.Val569Met substitution also

introduced a novel interaction with the p.Tyr110 residue, altering the binding pocket further (Figure 2E). The quantitative and qualitative alterations of the binding pocket (detailed in Supp. Figure S4) are most likely responsible for the slow-down of catalytic reactions and changes in the substrate binding affinity.Here we describe the first human *CRAT* sequence variants associated with a severe mitochondrial disorder that also shows carnitine acetyltransferase deficiency. This biochemical deficiency (MIM# 606175) has been previously observed in two sporadic cases of mitochondrial encephalopathy that are clinically reminiscent of Leigh syndrome (Didonato, Rimoldi, Moise, Bertagnoglio, & Uziel, 1979; Przyrembel, 1987) and that present RC defects (Przyrembel, 1987). In contrast to those two cases, which were not screened for DNA molecular diagnosis, our results demonstrate that the observed aberrant carnitine acetyltransferase function is caused by a primary *CRAT* genetic defect.

Recently, a single *CRAT* homozygous variant (p.Arg321His) has been described in a sporadic case of neurodegeneration with brain iron accumulation (Drecourt et al., 2018). In contrast to p.Arg321His, which is in the periphery of the CRAT protein structure and was proposed to affect CRAT protein stability (Drecourt et al., 2018), p.Tyr110Cys and p.Val569Met are located in the substrate binding area of the protein and damage the CRAT enzymatic functions. While multiple studies reported site-directed mutagenesis analyses to explore the basis of acyl-CoA selectivity in the carnitine acetyltransferase enzyme (see Cordente et al., 2006 and references therein), here we first characterized the kinetic properties and the substrate selectivity of CRAT variations found in the human population. In particular, we found that both p.Tyr110Cys and p.Val569Met retained less than one third of wild-type activity toward acetyl-CoA, and that p.Val569Met caused an analogous enzymatic impairment also toward propionyl-CoA and octanoyl-CoA. In addition to the increased level of

plasmatic short-chain acyl-CoAs in the proband, another evidence suggests that the two CRAT variations cannot fulfil the physiological function of the wild-type protein: the activity of the variant enzymes toward short-chain acyl-CoAs (the CRAT specific substrates) is lower than the wild-type activity toward the medium-chain acyl-CoA (a nonspecific and nonphysiological substrate of CRAT).

Albeit further studies are required to assess the neurometabolic consequences of CRAT defects, multiple literature findings suggest the importance of the ubiquitous CRAT protein for mitochondrial energy production. In particular, while the carnitine palmitoyltransferases CPT1 and CPT2 permit the import of long-chain fatty acyl-CoAs into the mitochondrial matrix for lipid β-oxidation (Wanders, Ruiter, Ijlst, Waterham, & Houten, 2010), a known cellular function of CRAT is exerted in the opposite direction, i.e. buffering the overload of mitochondrial acetyl-CoA that occurs when substrate oxidation exceeds energy demand (Seiler et al., 2014). Indeed, skeletal-muscle specific *Crat* knockout (KO) mice are subject to the over-accumulation of mitochondrial acetyl-CoA, which causes an inhibiting effect on pyruvate dehydrogenase (PDH) (Fisher-Wellman et al., 2015; Muoio et al., 2012), the reduction of oxygen consumption rates (Seiler et al., 2015), and the hyper-acetylation of multiple mitochondrial proteins, including subunits of PDH and RC complexes (Davies et al., 2016). Similar results were observed in another mouse model, in which *Crat* was selectively KO in a subset of hypothalamic neurons (Reichenbach et al., 2018). Since Crat deficiency in the skeletal muscle compromises the metabolic flexibility of the entire organism (Muoio et al., 2012) and Crat deficiency in hypothalamic AgRP neurons is sufficient to alter peripheral nutrient partitioning and liver metabolism (Reichenbach et al., 2018), one might speculate that germline carnitine acetyltransferase deficiency can even more severely damage the entire

organism (Supp. Figure S5). It will be most interesting to establish a whole-body or whole-brain mouse *Crat* KO model to explore the pathogenic phenotype of CRAT germline variants. In fact, the few studies conducted on human CRAT-deficient cells showed a generic role of CRAT in the resistance to oxidative stress (Sharma et al., 2013), and in the protection from mitochondrial dysfunction and apoptosis (Song, Kang, Yoon, Chun, & Jin, 2017). In conclusion, having shown that the catalytic dysfunction of the carnitine acetyltransferase enzyme is due to *CRAT* sequence variants in a case of Leigh syndrome, coherently with the importance of this enzymatic activity for mitochondrial energy production in health and disease, we propose that *CRAT* should be now screened in other human mitochondrial-related phenotypes than NBIA.

ACKNOWLEDGMENTS

DISCLOSURE STATEMENT

The authors declare no conflict of interest.

REFERENCES

Bloisi, W., Colombo, I., Garavaglia, B., Giardini, R., Finocchiaro, G., & Didonato, S. (1990). Purification and properties of carnitine acetyltransferase from human liver. *European Journal of Biochemistry*, *189*(3), 539–546. doi: 10.1111/j.1432-1033.1990.tb15520.x

Cordente, A. G., López-Viñas, E., Vázquez, M. I., Gómez-Puertas, P., Asins, G., Serra, D., & Hegardt, F. G. (2006). Mutagenesis of specific amino acids converts carnitine acetyltransferase into carnitine palmitoyltransferase. *Biochemistry*, *45*(19), 6133–6141. doi: 10.1021/bi0602664

Davies, M. N., Kjalarsdottir, L., Thompson, J. W., Dubois, L. G., Stevens, R. D., Ilkayeva, O. R., … Muoio, D. M. (2016). The Acetyl Group Buffering Action of Carnitine Acetyltransferase Offsets Macronutrient-Induced Lysine Acetylation of Mitochondrial Proteins. *Cell Reports*, *14*(2), 243–254. doi: 10.1016/j.celrep.2015.12.030

Didonato, S., Rimoldi, M., Moise, A., Bertagnoglio, B., & Uziel, G. (1979). Fatal ataxic encephalopathy and carnitine acetyltransferase deficiency: a functional defect of pyruvate oxidation? *Neurology*, *29*(12), 578–583. doi: 10.1212/WNL.29.12.1578

Drecourt, A., Babdor, J., Dussiot, M., Petit, F., Goudin, N., Garfa-Traoré, M., … Rötig, A. (2018). Impaired Transferrin Receptor Palmitoylation and Recycling in Neurodegeneration with Brain Iron Accumulation. *The American Journal of Human Genetics*, *102*(2), 266–277. doi: 10.1016/j.ajhg.2018.01.003

Fisher-Wellman, K. H., Lin, C.-T., Ryan, T. E., Reese, L. R., Gilliam, L. A. A., Cathey, B. L., … Neufer, P. D. (2015). Pyruvate dehydrogenase complex and nicotinamide nucleotide transhydrogenase constitute an energy-consuming redox circuit. *Biochemical Journal*, *467*(2), 271–280. doi: 10.1042/BJ20141447

Jogl, G., Hsiao, Y. S., & Tong, L. (2004). Structure and function of carnitine acyltransferases. *Annals of the New York Academy of Sciences*, *1033*, 17–29. doi: 10.1196/annals.1320.002

Lake, N. J., Compton, A. G., Rahman, S., & Thorburn, D. R. (2016). Leigh syndrome: One disorder, more than 75 monogenic causes. *Annals of Neurology*, *79*(2), 190–203. doi: 10.1002/ana.24551

Muoio, D. M., Noland, R. C., Kovalik, J. P., Seiler, S. E., Davies, M. N., Debalsi, K. L., … Mynatt, R. L. (2012). Muscle-specific deletion of carnitine acetyltransferase compromises glucose tolerance and metabolic flexibility. *Cell Metabolism*, *15*(5), 764–777. doi: 10.1016/j.cmet.2012.04.005

Przyrembel, H. (1987). Therapy of mitochondrial disorders. *Journal of Inherited Metabolic Disease*, *10*, 129–146. doi: 10.1007/BF01812853

Rahman, S., Blok, R. B., Dahl, H. H. M., Danks, D. M., Kirby, D. M., Chow, C. W., … Thorburn, D. R. (1996). Leigh syndrome: Clinical features and biochemical and DNA abnormalities. *Annals of Neurology*, *39*(3), 343–351. doi: 10.1002/ana.410390311

Ramsay, R. R., & Zammit, V. A. (2004). Carnitine acyltransferases and their influence on CoA pools in health and disease. *Molecular Aspects of Medicine*, *25*(5–6), 475–493. doi: 10.1016/j.mam.2004.06.002

Reichenbach, A., Stark, R., Mequinion, M., Denis, R. R. G., Goularte, J. F., Clarke, R. E., … Andrews, Z. B. (2018). AgRP Neurons Require Carnitine Acetyltransferase to Regulate Metabolic Flexibility and Peripheral Nutrient Partitioning. *Cell Reports*, *22*(7), 1745–1759. doi: 10.1016/j.celrep.2018.01.067

Ruhoy, I. S., & Saneto, R. P. (2014). The genetics of Leigh syndrome and its implications for clinical practice and risk management. *Application of Clinical Genetics*, *7*, 221–234. doi: 10.2147/TACG.S46176

Schaefer, J., Jackson, S., Taroni, F., Swift, P., & Turnbull, D. M. (1997). Characterisation of carnitine palmitoyltransferases in patients with a carnitine palmitoyltransferase deficiency: Implications for diagnosis and therapy. *Journal of Neurology Neurosurgery and Psychiatry*, *62*(2), 169–176. doi: 10.1136/jnnp.62.2.169

Seiler, S. E., Koves, T. R., Gooding, J. R., Wong, K. E., Stevens, R. D., Ilkayeva, O. R., … Muoio, D. M. (2015). Carnitine Acetyltransferase Mitigates Metabolic Inertia and Muscle Fatigue during Exercise. *Cell Metabolism*, *22*(1), 65–76. doi: 10.1016/j.cmet.2015.06.003

Seiler, S. E., Martin, O. J., Noland, R. C., Slentz, D. H., DeBalsi, K. L., Ilkayeva, O. R., … Muoio, D. M. (2014). Obesity and lipid stress inhibit carnitine acetyltransferase activity. *Journal of Lipid Research*, *55*(4), 635–644. doi: 10.1194/jlr.M043448

Sharma, S., Sun, X., Agarwal, S., Rafikov, R., Dasarathy, S., Kumar, S., & Black, S. M. (2013). Role of carnitine acetyl transferase in regulation of nitric oxide

signaling in pulmonary arterial endothelial cells. *International Journal of Molecular Sciences*, *14*(1), 255–272. doi: 10.3390/ijms14010255

Sitheswaran, N., Price, N. T., & Ramsay, R. R. (2005). The G553M mutant of peroxisomal carnitine octanoyltransferase catalyses acetyl transfer and acetyl-CoA hydrolysis. *Monatshefte Fur Chemie*, *136*(8), 1341–1347. doi: 10.1007/s00706-005-0293-z

Song, J., Kang, Y.-H., Yoon, S., Chun, C.-H., & Jin, E.-J. (2017). HIF-1α:CRAT:miR-144-3p axis dysregulation promotes osteoarthritis chondrocyte apoptosis and VLCFA accumulation. *Oncotarget*, *8*(41), 69351–69361. doi: 10.18632/oncotarget.20615

Wanders, R. J. A., Ruiter, J. P. N., Ijlst, L., Waterham, H. R., & Houten, S. M. (2010). The enzymology of mitochondrial fatty acid beta-oxidation and its application to follow-up analysis of positive neonatal screening results. *Journal of Inherited Metabolic Disease*, *33*(5), 479–494. doi: 10.1007/s10545-010-9104-8

Figures

Figure 1. Detection and effect of *CRAT* missense variants in the proband-derived cells.

(A) Trio-WES based detection of compound heterozygous variants, reported as the "Integrative Genome Viewer" output, and their location along the *CRAT* gene structure. (**B**) Gel electrophoresis and (**C**) Sanger sequencing of PCR products obtained from the fibroblast-derived cDNA shows no RNA-length alterations and biallelic gene expression. Arrows indicate the location of PCR

primer pairs along the gene structure. (**D**) Western-blot of fibroblast lysates.
(**E**) Example output of the spectrophotometric assays conducted on fibroblast lysates (one million cells) using the DTNB method and measuring the Absorbance at 412 nm (A_{412}) for two minutes at the steady-state. Carnitine was added for the activity assays of carnitine acetyltransferase and oxaloacetate for the activity assays of citrate synthase (CS). (**F**) CRAT activity normalized to CS activity. Both enzymatic activities are measured as $nmol \times min^{-1} \times 10^6$ cells. Data are presented as mean+SE of four independent experiments. ***: p-value <0.05, nonparametric Wilcoxon two-tailed test between proband and control.
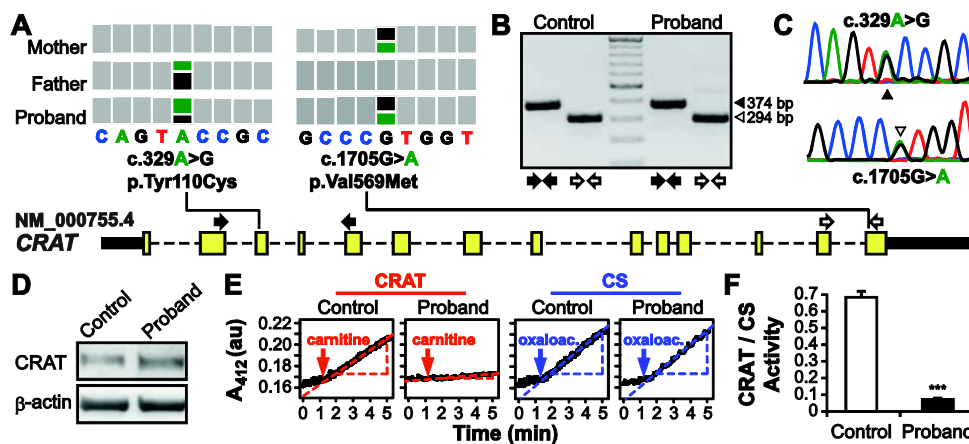
Figure 2. Functional and structural consequences of *CRAT* missense variants.

(**A**) Enzymatic activities of recombinant-purified CRAT proteins, measured using the DTNB method, at different concentrations of acetyl-CoA (C2), propionyl-CoA (C3) and octanoyl-CoA (C8); Michaelis-Menten (MM). (**B**) Maximum activity rate (V_{max}) and (**C**) MM constant K_m of recombinant-purified CRAT proteins. MM parameter estimations were conducted in GraphPad Prism. Data are presented as mean+SE of at least three independent experiments. ***: Non-overlapping 95% confidence

intervals between CRAT protein variations and wild-type. (**D**) Complete CRAT protein structure (PDB Identifier 1nm8). Amino acids of interest and acetylcarnitine are indicated in mesh and stick representation, respectively. (**E**) CRAT amino acids contributing to the binding pocket (<4Å from acyl groups or carnitine) are reported in surface representation in the wild-type protein (left) and in each remodeled variant protein (right). Sticks indicate acetyl-CoA (white), propionyl-CoA (grey) and octanoyl-CoA (black).
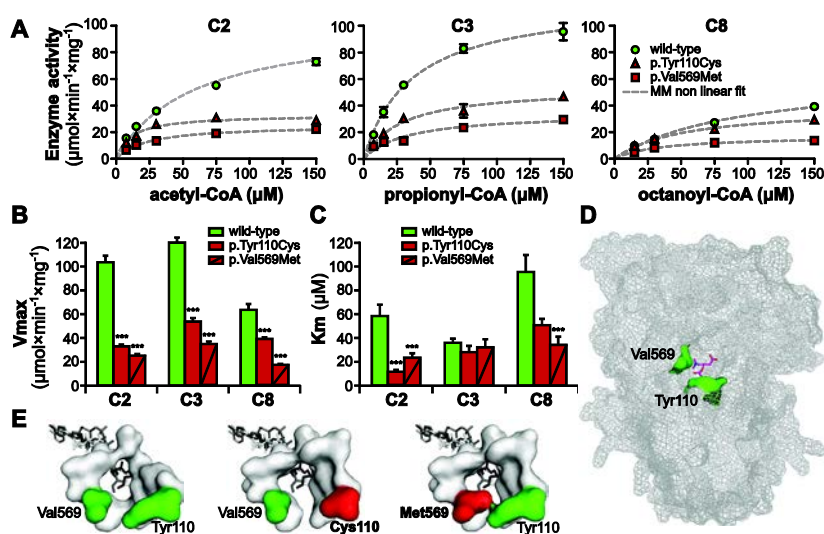
Supplementary Material and Methods

Case description

The proband is a 9-year-old only child of unrelated healthy parents. The family history was unremarkable. She was born post-term (41+4 weeks) after an uneventful pregnancy. Birth parameters were the normal range (weight: 2.9 Kg, height: 50 cm, OFC: 34 cm, APGAR: 9). In the firsts months feeding difficult was referred. Starting from five months of age, she presented subacute psychomotor regression, including microcephaly (<3rd percentile), reduced spontaneous motility, generalized hypotonia, poor eye contact, dysphagia, loss of postural control and hypertonic seizures. She also showed epileptic breathing abnormalities with multiple apneic and desaturation episodes that reached 36%. In the following years, clinical conditions progressively worsened into tetraparesis with extrapyramidal signs, dystonic postures involving both upper and lower limbs, failure to thrive (weight and length < 3rd percentile) and loss of swallowing ability. Early and periodic EEG screenings showed multifocal epileptiform abnormalities and poorly organized cerebral activity. A single MRI, conducted when she was six months of age, disclosed T2 hyperintensities in subthalami, substantia nigra, putamen, globus pallidus and periaqueductal gray matter, and a prominent lactate double peak. Quadriceps muscle biopsy was performed at nine months of age. Biochemical analysis, conducted in two different hospitals on biopsy-deriving muscle homogenates, showed mitochondrial respiratory chain defects that ranged from combined mitochondrial respiratory chain deficiency to isolated complex I deficiency, while normal activities were observed in cultured fibroblasts (Supp. Table 1). Initial metabolic workup showed high level of glucose (155 mg/dl, normal range 45-76), high level of triglycerides (373 mg/dl, normal range 64-122) and cholesterol (241 mg/dl, normal range <180), elevated level of lactate (up to 5605 μmol/l, normal range 800-2100) and low level of carnitine (5 μmol/l, normal range 22-47), which was improved after carnitine supplementation. A non-reiterated increase in the blood level was sporadically observed for the following metabolites: pyruvate, fumarate, malate, 2-oxoglutarate, 3-hydroxybutyrate. At regular follow-ups, altered values essentially regarded blood lactate level (2378 μmol/l, normal range 800-2100) and slightly low oxygen pressure (69 mm/Hg, normal range 70-100). Tandem mass spectrometry analysis of blood acylcarnitine, performed at six years of age, showed increase in short-chain acylcarnitines, while medium-chain and long-chain acylcarnitines were in the normal ranges (Supp. Table S2).

WES data production and analysis

Whole exome sequencing (WES) was performed using the Exome Capture Agilent V5+UTRs (71Mb) kit for library preparation and exome enrichment according to the manufacturer's instructions. Sequencing was conducted on the Illumina Genome Analyzer HiSeq2500 in paired-end mode, with a read length of 2x100bp, to generate at least 7 Gb per sample. Reads were filtered for sequencing quality and aligned to the human reference genome sequence (UCSC hg19, NCBI build 37.3) via the BWA program (Li & Durbin, 2009). Sequence variants were detected and annotated using the GATK toolkit (McKenna et al., 2009), and the VEP program (McLaren et al., 2010), respectively. The resulting variants were retained when the minor allele frequency was less than 0.005 in both the dbSNP146 database and in the ExAC database, or when variants were in genomic regions non-covered by those databases. Sequence variants located in coding

1

sequences and RNA splicing sites were then compared between the proband and her parents, using custom *Perl* scripts, under the following hypotheses of inheritance: dominant (*de novo* heterozygous variants) and recessive (homozygous variants and compound heterozygous variants). A visual inspection of the read alignments was performed to remove WES-mapping errors close to nucleotide repeats and other sequencing artifacts.

Fibroblast cultures and cDNA production

Primary dermal fibroblasts were cultured at 37 °C, 5% CO_2 in DMEM (Euroclone, ECM0103L), with 10% FBS (Euroclone, ECS0180L) and 1% antibiotics (Euroclone, ECM0010D). 90% confluent cells were harvested with 1% trypsin treatment (ECM0920D, Euroclone) and counted (Millipore, Scepter 2.0). Fibroblast RNA was extracted using the AURUM Total RNA Mini Kit (732-6820, Biorad) and retro-transcribed into cDNA using iScript Reverse Transcription Supermix for RT-qPCR kit (1708840, Biorad).

Immunoblotting

Fibroblasts (10^6 cells) were lysed in 100 µL of RIPA buffer and 20 µL of cell lysates were mixed with Laemmli buffer (161-074, Biorad) according to data-sheet and denatured at 95 °C for 5 min. After SDS-PAGE (TGX Stain-Free FastCast Acrylamide Kit, 12% #1610185 - Biorad), proteins were transferred onto a nitrocellulose membrane (88018, Thermo Fisher Scientific) and incubated with a blocking solution (5% milk-TBS). Proteins were probed with a primary anti-CRAT antibody (1:500, Rb-HPA022815 - Atlas Antibodies). The membrane was incubated in blocking solution overnight at 4 °C under shaking, washed (0.5 % Tween20-TBS) and incubated with secondary antibody (1:1000, AP307P, Goat Anti-Rb) in blocking solution for 2 h at room temperature under shaking. A mild stripping protocol (Stripping for reprobing, Abcam protocols) was used before incubating the membrane with a primary anti-β-actin antibody (1:1000 Ms-A5441, Sigma; secondary antibody AP308P, Goat Anti-Ms).

Enzymatic assays in fibroblasts

Citrate synthase activity was assessed using a spectrophotometric assay (Srere, 1969), and this assay was adapted for measuring carnitine acetyltransferase activity (Muoio et al., 2012). Briefly, fibroblasts ($2x10^6$ cells) were lysed with a cell lysis buffer (150 mM KCl, 25 mM Tris-HCl pH 8.00, 2 mM EDTA pH 8.00, 10 mM KH_2PO_4, 0.1% BSA and 30 µM digitonin) and the obtained samples were divided in two aliquots. Baseline measurements of absorbance (Varian spectrophotometer, Cary 50 UV-Vis) were obtained by incubating the first sample aliquot (1 min) in a reaction buffer (50 mM Tris-HCl pH 8.00, 1 mM EDTA pH 8.00, 0.1 mM DTNB, 0.45 mM acetyl-CoA). Citrate synthase activity was determined by measuring the rate of reduction of DTNB to TNB^{2-} (412 nm) by the free CoA-SH liberated from acetyl-CoA after adding 2mM oxaloacetic acid and monitoring for 5 min. Carnitine acetyltransferase was determined on the second sample aliquot using the same protocol and replacing 2 mM oxaloacetic acid by 2 mM L-carnitine. The absorbance variation in 2 min was used as a relative estimate of enzymatic activity.

Generation, expression and purification of recombinant CRAT proteins

A pET-21a(+) plasmid encoding the wild-type CRAT protein (NM_000755.4) was purchased from Genscript® (OHu15347). Each DNA sequence variant (c.1705G>A, p.Val569Met or c.329A>G, p.Tyr110Cys) was inserted by site-directed mutagenesis facilitated by *DpnI* selection. Briefly, 100 µg of the wild-type plasmid underwent PCR reactions using one of the following primer pairs (mutated site in bold):   forward 5'-TTCTTTGGTCCG**A**TGGTTCCGGATGG-3' and reverse 5'-CCATCCGGAACCA**T**CGGACCAAAGAA-3' for p.Val569Met; forward 5'-CGTACCTGCAGT**G**TCGTCAACCGGT-3' and reverse 5'-ACCGGTTGACGA**C**ACTGCAGGTACG-3' for p.Tyr110Cys. PCR products were incubated with 20 units of *DpnI* restriction enzyme (NEB R0176S) at 37 °C for 2 h to degrade wild-type plasmids, and enzyme inactivation was conducted at 80 °C for 20 min. Mutant PCR products (2 µl) were then used for transforming competent TOP10 *E. coli* cells, and the presence of each CRAT variant was confirmed by plasmid extraction followed by Sanger sequencing.

Escherichia coli Rosetta (DE3) cells were transformed with wild-type or mutant plasmids, in which CRAT proteins were expressed in frame with 6X-L-histidine-tag codons. After 12 h on selective LB agar plates, the transformed bacterial clones were cultured over-night in a liquid LB selective medium. The day after, bacterial cultures were diluted in fresh medium, grown to reach optical density 0.5 OD/ml and IPTG (1 mM) was added to induce CRAT expression. After 4 h, bacterial cells were collected by centrifugation and lysed with French press in a buffer solution containing imidazole (10 mM). After ultracentrifugation, total protein extracts were incubated with a nickel-charged resin (Profinity IMAC resin, #1560133). The nickel-charged resin was washed using buffers at increasing concentrations of imidazole to remove nonspecific-bounded proteins, and CRAT proteins were finally eluted using a 100 mM imidazole buffer solution. The purity of recombinant CRAT proteins was assessed by SDS-PAGE (TGX Stain-Free FastCast Acrylamide Kit, 12%, #161018, Biorad), while their concentrations were determined using two independent methods, i.e. Bradford Protein Assays and SDS-PAGE of multiple CRAT protein dilutions.

Catalytic properties of CRAT recombinant proteins

All acyl-CoA substrates were purchased from Sigma-Aldrich (acetyl-CoA, A2056; propionyl-CoA, P5397; octanoyl-CoA, O6877), dissolved in distilled water according to the manufacturer's instructions and diluted to the concentration required. CRAT specific activity was measured using the same enzymatic assay applied to fibroblasts. For each experiment the CRAT purified protein (100 ng) was mixed with the reaction buffer including the acyl-CoA (7.5-150 mM). Baseline absorbance was measured for 1 min. Reactions started by adding 2 mM L-carnitine in a total reaction volume 500 µl and were followed for 5 min. All reactions were conducted at the steady-state (linear increase of absorbance during time). CRAT specific activities (AS, µmol × min^{-1} × mg protein) were calculated as AS = $\Delta A \times \Delta t^{-1} \times \epsilon^{-1} \times l^{-1} \times$ vol × mg protein-^{1}, where $\Delta A \times \Delta t^{-1}$ is the variation of absorbance per minute (min^{-1}), ϵ is the extinction coefficient of TNB^{2-} (13.8 ml × µmol^{-1} × cm^{-1}), l is the path length (1 cm) and vol is the total reaction volume (ml).   CRAT   specific   activities   were   analyzed   using   GraphPad   Prism   5 (https://www.graphpad.com/scientific-software/prism)   to   verify   whether   they   fitted   a

Michaelis-Menten kinetic model and to calculate V_{max} and K_m, consequently.

Analysis and remodeling of CRAT protein structures

The PyMOL software was used to visualize the high-resolution crystallized structure of the wild-type CRAT protein (PDB ID 1nm8, resolution 1.6 Å) and to place substrates. The binding poses of substrates within this CRAT protein structure were generated by superimposition using a CRAT structure crystallized in complex with carnitine (PDB ID 1s5O, resolution 1.8 Å) and a mouse Crat structure crystallized in complex with acetyl-CoA (PDB ID 2h3p, resolution 2.2 Å). Acetylcarnitine position was derived by acetylating carnitine *in silico* using PyMOL. The structures of propionyl-CoA (http://www.rcsb.org/ligand/1VU) and octanoyl-CoA (http://www.rcsb.org/ligand/CO8) were fetched from PDB and superimposed over the acetyl-CoA structure. The 3D model of each variant CRAT protein was generated by *in silico* mutagenesis and protein structure remodeling according to the protocols described in (Pierri, Parisi, & Porcelli, 2010). One hundred steps of energy minimization were performed on mutant 3D models using the Chimera tool, and the correct 3D model packing was verified (Chimera and WhatIF). After having generated the overlap between all structures (proteins and substrates), amino acid residues at less than 4 Å from acyl groups or carnitine were selected in each CRAT 3D model (wild-type and variations) for comparative purposes.

Supplementary Tables

First Institute		Second Institute		
Activity *μmol× min^{-1} × g tissue*	**Muscle**	**Activity** *nmol × min^{-1}× mg protein*	**Muscle**	**Cultured fibroblasts**
Complex I	**22.6** (27.5-39.5)	**Complex I / CS**	**0.4** (13-28)	14.3 (10.7-26.0)
Complex II	0.72 (0.5-0.75)	**Complex II / CS**	32.3 (9-20)	7 (6.5-14.3)
Complex III	-	**Complex III / CS**	101 (70-130)	98 (70-120)
Complex IV	**0.85** (1.8-2.45)	**Complex IV / CS**	150 (130-250)	183 (95-150)
Complex V	-	**Complex V / CS**	264 (120-380)	123 (65-113)
CS	14.34 (7.8-10.9)	**CS**	168 (60-210)	203 (100-200)

Supplementary Table S1. Activities of mitochondrial respiratory chain complexes.

Values were recovered from the medical records obtained by two Neurological Institutes. Biochemical assays were conducted as described in (Trounce, Kim, Jun, & Wallace, 1996) for the first Institute, and as described in (Bugiani et al., 2004) for the second Institute. The latter reports the activities of complexes normalized to citrate synthase (CS) activity. Reference ranges are indicated in brackets.

Despite the difficulty in reproducing results from patient-derived tissue samples with OXPHOS deficiencies (Rodenburg, 2011), two independent Institutes found respiratory chain defects in the skeletal muscle of the proband. There are at least two major influencing factors that might explain the partial difference regarding the results on skeletal muscle. First, the two assay protocols are largely different for several aspects including substrates, substrate concentrations and buffer conditions. For example, the spectrophotometric Complex I assay is based on completely different reactions, i.e. the first Institute measured decylubiquinone decrease in absorbance at 272 minus 247 nm after adding NADH, while the second Institute measured NADH decrease in absorbance at 340 nm after adding coenzyme Q1. Further, the first Institute normalized the activities of Complexes per gram of tissue, while the second Institute per microgram of total proteins, and each Institute established its own reference ranges to which diagnostic test results are related. Second, the two Institutes analysed distinct slices of the same biopsy tissue that is a non-homogeneous source of cells and cell types, which might undergo non-homogeneous metabolic alterations. Finally, respiratory chain defects in the skeletal muscle, in presence of normal activities in fibroblasts, are coherent with an impairment of the respiratory chain that is secondary to other mitochondrial alterations.

Plasma Carnitine	Quantity (μM)	Reference range (μM)
Free	45.0	20.0 - 48.0
Short-chain esters	**12.3***	2.0 - 8.0
Medium- and long-chain esters	0.7	0.3 - 1.8
Total carnitine	58.0	25.0 - 62.0
Medium and long-chain esters / Total $\times$ 100	1.2	< 5.0

**Supplementary Table S2. Plasma free and esterified carnitines in the proband.**

The levels of plasma carnitine, measured using electrospray ionisation and tandem-mass spectrometry (ESI/MS/MS), were recovered from a medical record of the proband. *: The medical record specifies that the increased level of short-chain acylcarnitines depends on the level of acetylcarnitine, while the other acylcarnitines are quantitatively and qualitatively normal.

Substrate	K$_m$ (μM)		
	wild-type	p.Tyr110Cys	p.Val569Met
C2-CoA	58.0 ± 9.6	11.3 ± 2.0*	23.3 ± 3.8*
C3-CoA	36.0 ± 3.4	28.0 ± 5.4	32.1 ± 6.9
C8-CoA	95.4 ± 14.3	50.7 ± 5.4*	34.2 ± 6.9*

**Supplementary Table S3. K$_m$ values of CRAT proteins towards different substrates.**

Data are presented as mean±SE of at least three independent experiments. C2-CoA: acetyl-CoA; C3-CoA: propionyl-CoA; C8-CoA: octanoyl-CoA. *: Non-overlapping 95% confidence intervals between CRAT protein variations and wild-type.
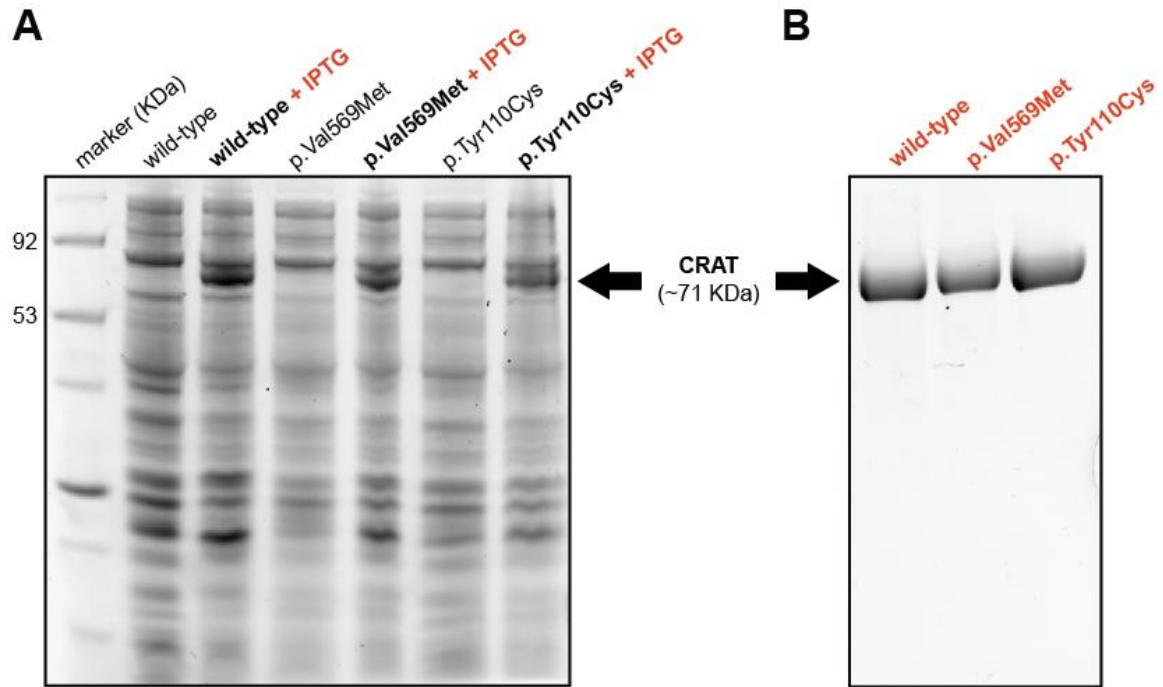
Supplementary Figures
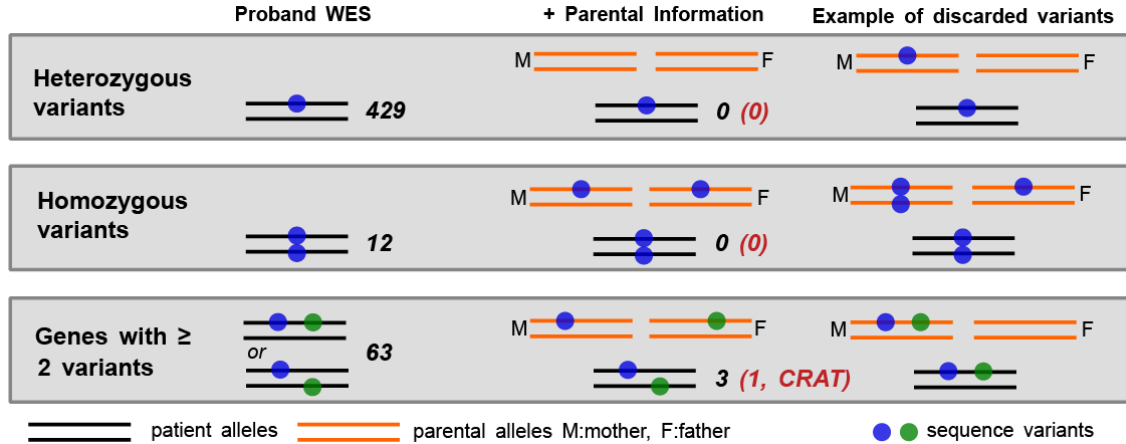
Supplementary Figure S1. *CRAT* **is the only candidate gene encoding a mitochondrial protein.**

Each row refers to a class of DNA sequence variants. Numbers refer to sequence variants detected in the patient before (first column) and after (second column) having considered the parental information for the selection of sequence variants. The third column indicates examples of allele combinations that could be discarded using parental information. The number of genes encoding mitochondria-targeted proteins are reported in brackets.
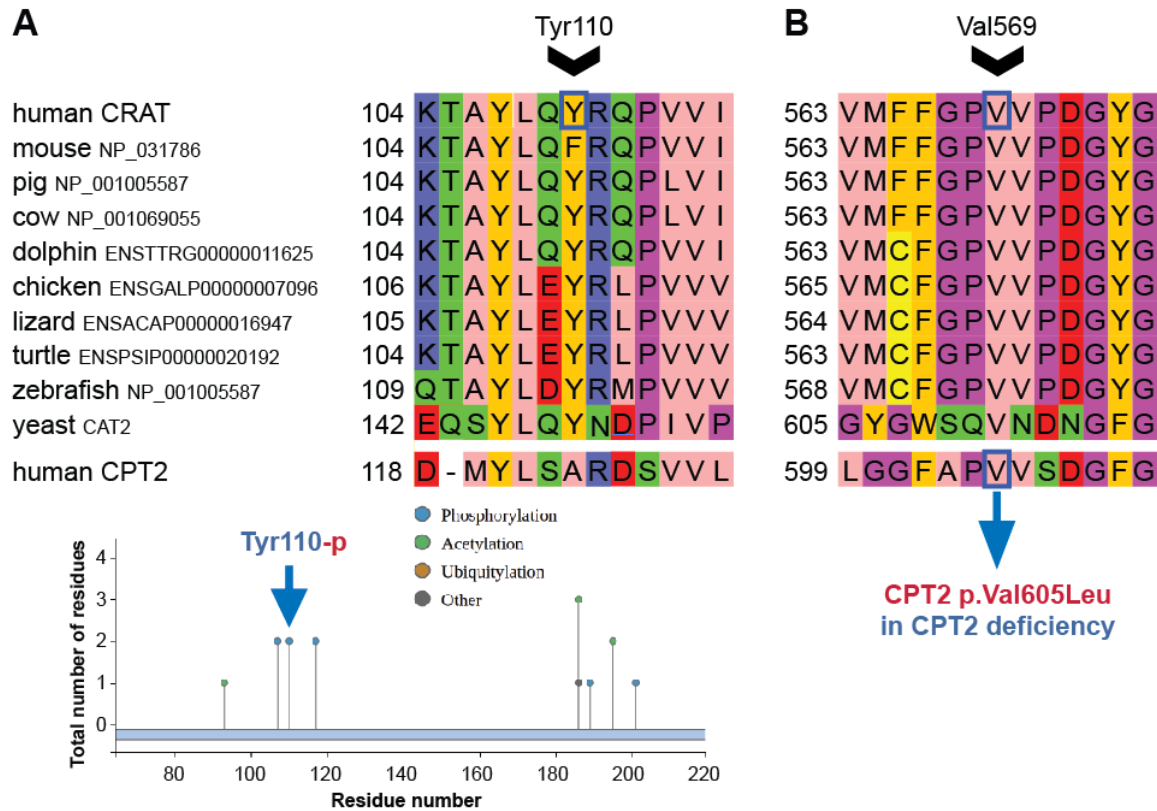
Supplementary Figure S2. CRAT p.Tyr110 and p.Val569 are evolutionary conserved.

(**A-B**) Multi-alignment of CRAT orthologous sequences deriving from the following species: *M. musculus* (mouse), *S. scrofa* (pig), *B. taurus* (cow), *T. truncatus* (dolphin), *G. gallus* (chicken), *A carolinensis* (lizard), *P. sinensis* (turtle), *D. rerio* (zebrafish) and *S. cerevisiae* (yeast). (**A**) The arrow indicates the phosphorylation of Tyr110 (Tyr110-p) detected in two experiments reported in the PhosphoSitePlus database (https://www.phosphosite.org/). (**B**) The arrow indicates evolutionary conservation between CRAT p.Val569 and CPT2 p.Val605 that hosts the amino acid substitution CPT2 p.Val605Leu responsible of CPT2 deficiency (Yasuno et al., 2008).

Supplementary Figure S3. Expression and purification of recombinant CRAT proteins.

(**A**) SDS-PAGE of bacterial lysates before and after the IPTG-induced expression of plasmids encoding the three recombinant CRAT proteins. (**B**) SDS-PAGE of recombinant-purified CRAT proteins.
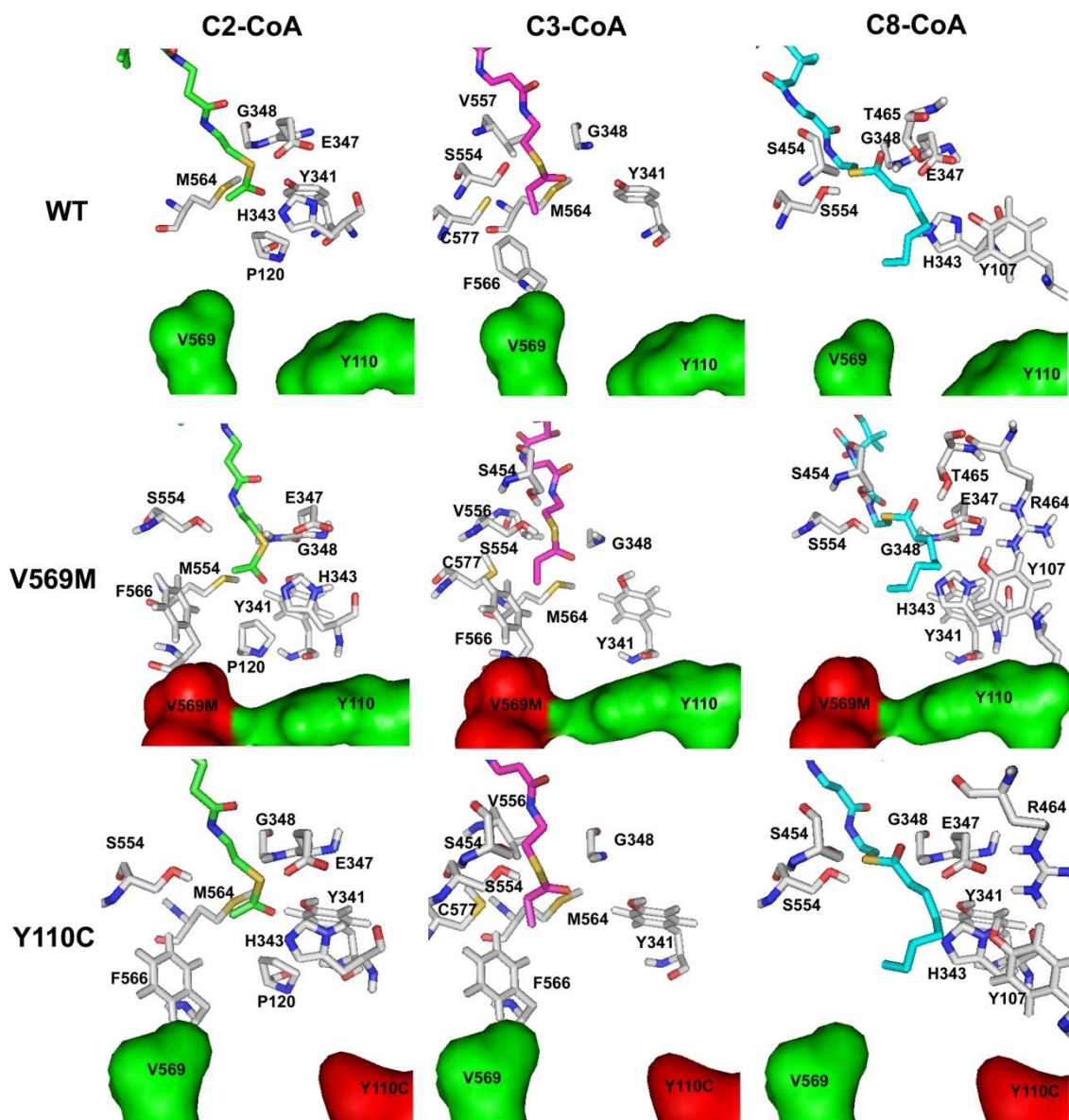
Supplementary Figure S4. CRAT amino-acid residues interacting with acyl groups.

Stick representation of CRAT amino-acid residues within 4 Å from each substrate (C2-CoA, green sticks, C3-CoA, magenta sticks, and C8-CoA, cyan sticks) are reported the wild-type protein structure (WT), in p.Val569Met protein structure (V569M) and in the p.Tyr110Cys protein structure (Y110C). Each CRAT variation shows qualitative and quantitative differences, compared to wild-type, in the amino-acid residues contributing to the binding of each substrate. Further, both CRAT variations introduce two novel amino-acid interactions, compared to wild-type, with acetyl-CoA (S554 ed F566) and with octanoyl-CoA (Y341 and R464), while only one novel amino-acid interaction with propionyl-CoA (S454). Thus, propionyl-CoA appears to be less susceptible than the other two substrates to a change in binding affinity (and then in K_m values) in CRAT variations compared to wild-type.
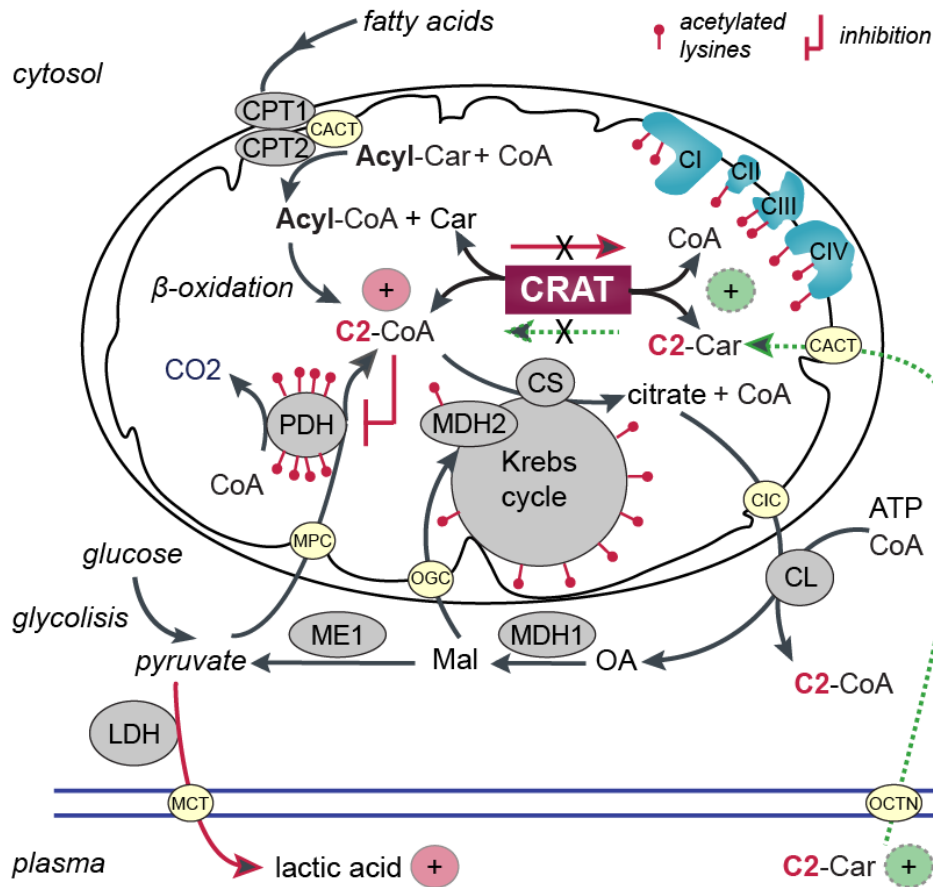
Supplementary Figure S5. CRAT-mediated buffering of mitochondrial acetyl moieties.

CRAT catalyses a reversible enzymatic reaction, whose direction is essentially driven by the concentration of substrates. Studies based on a skeletal-muscle *Crat* KO model demonstrated that, when the level of nutrients, i.e. glucose and fatty acids, exceeds the energy demand of the skeletal muscle, Crat lowers mitochondrial acetyl-CoA and regenerates free CoA (red arrow), which together disinhibit PDH (Muoio et al., 2012). Thus, the Crat-generated acetylcarnitine can temporary, and reversibly, stores acetyl moieties into mitochondria until acetyl-CoA lowers and the enzymatic reaction can occur in the opposite direction (green arrow) with the net effect of constantly fuel the Krebs cycle. Albeit acetyl-CoA can be exported out of mitochondria using the citrate shuttle (Palmieri, 2004), this route implies multiple enzymes, is ATP-consuming and, therefore, is expected to respond more slowly and more stably to the accumulation of mitochondrial acetyl-CoA than the Crat-mediated route. Further, mitochondrial protein acetylation is thought to be largely non-enzymatic and enabled by acetyl-CoA abundance (Baeza, Smallegan, & Denu, 2016). In this respect, additional studies of the skeletal-muscle *Crat* KO model showed that the over-accumulation of mitochondrial acetyl-CoA resulting from Crat deficiency causes the lysine hyperacetylation (red sticks) of multiple mitochondrial proteins (Davies et al., 2016), e.g. subunits of the PDH complex (Dld and Pdhb), Krebs cycle enzymes and multiple mitochondrial respiratory chain (RC) proteins, including Complex I subunits (Ndufa9

and Ndufs1). It is worth nothing that Leigh syndrome can be caused by primary defects of either DLD or NDUFA9 (MIM# 256000). Albeit the functional consequence of acetylation on each RC complex subunit is still largely unknown, blocking the lysine de-acetylation of mouse Ndufa9 can indeed cause a secondary impairment of the Complex I activity (Ahn et al., 2008). Taking together all these findings, one might speculate that also in the skeletal muscle of the proband the excess of mitochondrial acetyl-CoA due to carnitine acetyltransferase deficiency might cause the inhibition of the PDH activity and the secondary impairment of the RC function, the latter due to the lysine hyperacetylation of some RC subunits. This speculation is coherent with the excess of plasma lactate observed in the proband and it might also explain the normal RC function observed in the proband-derived fibroblasts, which are cells with a poor mitochondrial oxidative metabolism, and might not require the CRAT-mediated buffering of mitochondrial acetyl moieties. Albeit the only mouse *Crat* KO models are specific of skeletal muscle (Muoio et al., 2012) or hypothalamic AgRP neurons (Reichenbach et al., 2018), CRAT is an ubiquitous protein, thus it might be functionally relevant in other tissues than skeletal muscle. For example, liver is the major contributor to systemic acetylcarnitine during fasting (Xu et al., 2016) and liver β-oxidation of palmitoyl-CoA correlates with a strong increase in the Crat mRNA levels and with a reduction of plasma acetylcarnitine (Bjørndal et al., 2018; Lindquist et al., 2017). Further, acetylcarnitine, which is largely the most abundant plasma acylcarnitine (Giesbertz, Ecker, Haag, Spanier, & Daniel, 2015), can cross the blood brain barrier and induce a long-studied neuroprotective effect (Ferreira & Mckenna, 2017). Thus, CRAT might also facilitate a rapid influx of acetyl moietis from plasma to mitochondria *via* acetylcarnitine. If so, the excess of plasma acetylcarnitine observed in the proband might be explained by a reduced capability of CRAT deficient cells to transform acetylcarnitine. Contrary to acetylcarnitine, which is an oxoester, acetyl-CoA is a thioester, i.e. an extremely reactive donor substrate in transacetylation reactions (Yang & Drueckhammer, 2001). In this light, and since the proband is regularly supplemented with carnitine, the excess of plasma acetylcarnitine might simply reflect an excess of acetyl-CoA.

CACT, carnitine acylcarnitine translocase; CI-CIV, respiratory chain complexes; CIC, citrate carrier; CL, citrate lyase; CPT1, carnitine palmitoyltransferase 1; CPT2, Carnitine palmitoyltransferase 2; CRAT, carnitine acetyltransferase; CS, citrate synthase; LDH, lactate dehydrogenase; MCT, monocarboxylate transporter; MDH1, malate dehydrogenase 1; MDH2, Malate dehydrogenase 2; ME1, malic enzyme 1; MPC, mitochondrial pyruvate carrier; OCTN, organic cation transporter; OGC, malate/2-oxoglutarate carrier; PDH, pyruvate dehydrogenase.

Supplementary References

Ahn, B.-H., Kim, H.-S., Song, S., Lee, I. H., Liu, J., Vassilopoulos, A., … Finkel, T. (2008). A role for the mitochondrial deacetylase Sirt3 in regulating energy homeostasis. *Proceedings of the National Academy of Sciences*, *105*(38), 14447–14452. doi: 10.1073/pnas.0803790105

Baeza, J., Smallegan, M. J., & Denu, J. M. (2016). Mechanisms and Dynamics of Protein Acetylation in Mitochondria. *Trends in Biochemical Sciences*, *41*(3), 231–244. doi: 10.1016/j.tibs.2015.12.006

Bjørndal, B., Alterås, E. K., Lindquist, C., Svardal, A., Skorve, J., & Berge, R. K. (2018). Associations between fatty acid oxidation, hepatic mitochondrial function, and plasma acylcarnitine levels in mice. *Nutrition & Metabolism*, *15*, 10. doi: 10.1186/s12986-018-0241-7

Bugiani, M., Invernizzi, F., Alberio, S., Briem, E., Lamantea, E., Carrara, F., … Zeviani, M. (2004). Clinical and molecular findings in children with complex I deficiency. *Biochimica et Biophysica Acta - Bioenergetics*, *1659*, 136–147. doi: 10.1016/j.bbabio.2004.09.006

Davies, M. N., Kjalarsdottir, L., Thompson, J. W., Dubois, L. G., Stevens, R. D., Ilkayeva, O. R., … Muoio, D. M. (2016). The Acetyl Group Buffering Action of Carnitine Acetyltransferase Offsets Macronutrient-Induced Lysine Acetylation of Mitochondrial Proteins. *Cell Reports*, *14*(2), 243–254. doi: 10.1016/j.celrep.2015.12.030

Ferreira, G. C., & Mckenna, M. C. (2017). L-Carnitine and Acetyl-L-carnitine Roles and Neuroprotection in Developing Brain. *Neurochemical Research*, *42*(6), 1661–1675. doi: 10.1007/s11064-017-2288-7

Giesbertz, P., Ecker, J., Haag, A., Spanier, B., & Daniel, H. (2015). An LC-MS / MS method to quantify acylcarnitine species including isomeric and odd-numbered forms in plasma and tissues. *The Journal of Lipid Research*, *56*, 2029–2039. doi: 10.1194/jlr.D061721

Li, H., & Durbin, R. (2009). Fast and accurate short read alignment with Burrows-Wheeler transform. *Bioinformatics*, *25*(14), 1754–1760. doi: 10.1093/bioinformatics/btp324

Lindquist, C., Bjørndal, B., Rossmann, C. R., Tusubira, D., Svardal, A., Røsland, G. V., … Berge, R. K. (2017). Increased hepatic mitochondrial FA oxidation reduces plasma and liver TG levels and is associated with regulation of UCPs and APOC-III in rats. *Journal of Lipid Research*, *58*(7), 1362–1373. doi: 10.1194/jlr.M074849

McKenna, A., Aaron, M., Banks, E., Sivachenko, A., Cibulskis, K., Kernytsky, A., … DePristo, M. A. (2009). The Genome Analysis Toolkit: A MapReduce framework for analyzing next-generation DNA sequencing data. *Genome Research*, *20*, 254–260. doi: 10.1101/gr.107524.110.20

McLaren, W., Pritchard, B., Rios, D., Chen, Y., Flicek, P., & Cunningham, F. (2010). Deriving the consequences of genomic variants with the Ensembl API and SNP Effect Predictor. *Bioinformatics*, *26*(16), 2069–2070. doi: 10.1093/bioinformatics/btq330

Muoio, D. M., Noland, R. C., Kovalik, J. P., Seiler, S. E., Davies, M. N., Debalsi, K. L., … Mynatt, R. L. (2012). Muscle-specific deletion of carnitine acetyltransferase compromises

glucose tolerance and metabolic flexibility. *Cell Metabolism*, *15*(5), 764–777. doi: 10.1016/j.cmet.2012.04.005

Palmieri, F. (2004). The mitochondrial transporter family (SLC25): physiological and pathological implications. *Pflugers Archiv : European Journal of Physiology*, *447*(5), 689–709. doi: 10.1007/s00424-003-1099-7

Pierri, C. L., Parisi, G., & Porcelli, V. (2010). Computational approaches for protein function prediction: a combined strategy from multiple sequence alignment to molecular docking-based virtual screening. *Biochimica et Biophysica Acta*, *1804*(9), 1695–1712. doi: 10.1016/j.bbapap.2010.04.008

Reichenbach, A., Stark, R., Mequinion, M., Denis, R. R. G., Goularte, J. F., Clarke, R. E., … Andrews, Z. B. (2018). AgRP Neurons Require Carnitine Acetyltransferase to Regulate Metabolic Flexibility and Peripheral Nutrient Partitioning. *Cell Reports*, *22*(7), 1745–1759. doi: 10.1016/j.celrep.2018.01.067

Rodenburg, R. J. T. (2011). Biochemical diagnosis of mitochondrial disorders. *Journal of Inherited Metabolic Disease*, *34*(2), 283–292. doi: 10.1007/s10545-010-9081-y

Srere, P. A. (1969). Citrate synthase. *Methods in Enzymology*, *13*, 3–11. doi: 10.1016/0076-6879(69)13005-0

Trounce, I. A., Kim, Y. L., Jun, A. S., & Wallace, D. C. (1996). Assessment of mitochondrial oxidative phosphorylation in patient muscle biopsies, lymphoblasts, and transmitochondrial cell lines. *Methods in Enzymology*, *264*, 484–509. doi: doi.org/10.1016/S0076-6879(96)64044-0

Xu, G., Hansen, J. S., Zhao, X. J., Chen, S., Hoene, M., Wang, X. L., … Plomgaard, P. (2016). Liver and Muscle Contribute Differently to the Plasma Acylcarnitine Pool During Fasting and Exercise in Humans. *The Journal of Clinical Endocrinology & Metabolism*, *101*(12), 5044–5052. doi: 10.1210/jc.2016-1859

Yang, W., & Drueckhammer, D. G. (2001). Understanding the Relative Acyl-Transfer Reactivity of Oxoesters and Thioesters: Computational Analysis of Transition State Delocalization Effects. *Journal of the American Chemical Society*, *123*(44), 11004–11009. doi: 10.1021/ja010726a

Yasuno, T., Kaneoka, H., Tokuyasu, T., Aoki, J., Yoshida, S., Takayanagi, M., … Saito, T. (2008). Mutations of carnitine palmitoyltransferase II (CPT II) in Japanese patients with CPT II deficiency. *Clinical Genetics*, *73*(5), 496–501. doi: 10.1111/j.1399-0004.2008.00986.x